A Study of H_2O_2 with Threshold Photoelectron Spectroscopy (TPES) and Electronic Structure Calculations: Re-determination of the first Adiabatic Ionization Energy (AIE)

by

Luca Schio[(a)], Michele Alagia[(a)], Antonio A. Dias[(b)], Stefano Falcinelli[(c)], Vitali Zhaunerchyk[(d)], Edmond P.F.Lee[(e,f)], Daniel K.W.Mok[(f)], John M. Dyke[(e)*] and Stefano Stranges[(g)*],

(a) IOM-CNR Tasc Laboratory, SS-14, Km 163.5, Area Science Park, 34149 Basovizza, Trieste, Italy
(b) LIBPhys-UNL, Laboratory for Instrumentation, Biomedical Engineering and Radiation Physics; Departamento de Física, Faculdade de Ciências e Tecnologia, Universidade NOVA de Lisboa, Caparica, Portugal
(c) Dipartimento di Ingegneria Civile ed Ambientale, Università di Perugia, 06125 Perugia, Italy
(d) Department of Physics, University of Gothenburg, 41296 Gothenburg, Sweden
(e) School of Chemistry, University of Southampton, Highfield, Southampton SO17 1BJ, UK
(f) Department of Applied Biology and Chemical Technology, The Hong Kong Polytechnic University, Hung Hom, Hong Kong
(g) Department of Chemistry and Drug Technologies, Sapienza University, P.le A. Moro 5, 00185 Rome, Italy, and IOM-CNR, Tasc Laboratory, SS-14, Km 163.5, Area Science Park, 34149 Basovizza, Trieste, Italy

*to whom correspondence should be addressed

Abstract

In this work hydrogen peroxide has been studied with threshold photoelectron (TPE) spectroscopy and photoelectron (PE) spectroscopy**.** The TPE spectrum has been recorded in the 10.0-21.0 eV ionization energy region, and the PE spectrum has been recorded at 21.22 eV photon energy. Five bands have been observed which have been assigned on the basis of UCCSD(T)-F12/VQZ-F12 and IP-EOM CCSD calculations.

Vibrational structure has only been resolved in the TPE spectrum of the first band, associated with the $\tilde{X}\ ^2B_g\ H_2O_2^+ \leftarrow \tilde{X}\ ^1A\ H_2O_2$ ionization, on its low energy side. This structure is assigned with the help of harmonic Franck Condon factor calculations which use the UCCSD(T)-F12a/VQZ-F12 computed adiabatic ionization energy (AIE), and UCCSD(T)-F12a/VQZ-F12 computed equilibrium geometric parameters and harmonic vibrational frequencies for the H_2O_2 $\tilde{X}^1A$ state and the $H_2O_2^+$ $\tilde{X}^2B_g$ state. These calculations show that the main vibrational structure on the leading edge of the first TPE band is in the O-O stretching mode (ω_3) and the HOOH deformation mode (ω_4), and comparison of the simulated spectrum to the experimental spectrum gives the first AIE of H_2O_2 as (10.685 ± 0.005) eV and ω_4 = (850 ± 30) and ω_3 =(1340 ±30) cm^{-1} in the $\tilde{X}^2B_g$ state of $H_2O_2^+$.

Contributions from ionization of vibrationally excited levels in the torsion mode have been identified in the TPE spectrum of the first band and the need for a vibrationally resolved TPE spectrum from vibrationally cooled molecules, as well as higher level Franck-Condon factors than performed in this work, is emphasized.

Introduction

Hydrogen peroxide, H_2O_2, plays important roles in the earth's atmosphere (1) and in combustion (2,3), as well as in oxidation reactions (4) and biological processes (5). It has also proven to be a very interesting molecule for selective excitation studies of unimolecular decay dynamics (6-8) and it is one of the simplest molecules which displays a large-amplitude internal torsional vibration. It is considered an important prototypical molecule as the simplest chiral molecule (9-11), exhibiting "transient" chirality due to the rapid tunnelling through the double well torsional barrier in the ground state, which allows a rapid racemization between the two enantiomeric forms ($g^{\pm}$).

H_2O_2 is formed in the troposphere and stratosphere , via the reaction:

$$HO_2 + HO_2 + M \rightarrow H_2O_2 + O_2 + M \qquad (1)$$

which is also important in determining the third explosion limit in hydrogen/oxygen combustion (12). The rate of this reaction depends on the overall pressure and water concentration. H_2O_2 is soluble in cloud droplets and can be removed from the atmosphere by rain. It can also be removed by reaction with OH and photolysis:

$$OH + H_2O_2 \rightarrow H_2O + HO_2 \qquad (2)$$

$$H_2O_2 + h\nu \rightarrow OH + OH \qquad (3)$$

where (2) usually dominates over (3). In the stratosphere H_2O_2 is an important reservoir for HO_2 and OH, produced by photolysis of H_2O_2, and these HO_x radicals contribute to catalytic cycles (e.g. the ClO_x and NO_x cycles), resulting in increased ozone removal.

Spectroscopic studies on H_2O_2 in the gas-phase have been made in the infrared, far-infrared and microwave regions (13-17). The rotationally resolved infrared spectrum has been analyzed and rotational constants have been derived which are consistent with a C_2 ground state structure with a dihedral angle of 119.8°, and O-O = 1.475 Å, O-H = 0.950 Å and $\angle$OOH = 94.8° (13) (this is essentially an r_0 structure; see the Supplementary Information, SI). A high resolution study of H_2O_2 in the far infrared region (14) derived barrier heights of (387.07 $\pm$ 0.20) and (2562.8 $\pm$ 60.0) cm^{-1} for the trans and cis barriers in H_2O_2.

There have been a number of studies of H_2O_2 with photoelectron spectroscopy (PES) (18-20), and electron impact (21) and photoionization mass spectrometry (PIMS) (22). At a photon energy of 21.22 eV, the PE spectrum shows five bands. The first two bands are partially overlapped as are the fourth and fifth bands, with only the third band not overlapped by other bands. The first band corresponds to removal of an electron from the highest occupied molecular orbital in H_2O_2 which consists of an antisymmetric combination of

atomic oxygen 2p orbitals on each centre, and is essentially an anti-bonding π-molecular orbital with respect to the O-O bond. The dihedral angle increases significantly on ionization from approximately 120° in the neutral to 180° in the ground state of the cation, which has a C_{2h} trans planar geometry (23). The two most recent PE studies have been made by Ashmore and Burgess (19) and Brown (20). The first adiabatic ionization energy (AIE) and the first vertical ionization energy (VIE) have been reported in ref.(19) as (10.62 ± 0.02) and (11.70 ± 0.02) eV, and in ref. (20) as (10.54 ± 0.02) and (11.51 ± 0.02) eV. In both studies, some poorly resolved vibrational structure has been observed on the leading edge of the first band with average vibrational separations of (1050 ± 30) (19) and (1080 ± 50) cm^{-1} (20) respectively, increased from the value of the O-O stretching mode in the ground state neutral of 878 cm^{-1} (24). The first AIE has been derived in a PIMS study as (10.631 ± 0.007) eV (22). The first two photoelectron bands of H_2O_2 have also been simulated using geometrical parameters and vibrational constants obtained for the ground state of H_2O_2 and the two lowest states of $H_2O_2^+$, obtained on one-electron ionization from the neutral (23). The harmonic oscillator model was used to obtain vibrational wavefunctions in each state, from which Franck-Condon factors were computed. Unfortunately, as the electronic wavefunctions for the neutral and ionic states were only obtained at the Hartree-Fock SCF level, the geometric parameters and vibrational constants in each state are inaccurate; for example in the neutral ground state O-O and O-H equilibrium bond lengths are too small and the O-O and O-H stretching frequencies are too high when compared with experimental values. Hence the results of these calculations, although providing a useful guide to the expected vibrational envelopes, cannot be used for a detailed comparison with a vibrationally resolved experimental spectrum.

The objective of this work is to obtain a higher resolution photoelectron spectrum of H_2O_2 than has previously been recorded, by using threshold photoelectron spectroscopy (TPES). Where vibrational structure is observed, *ab initio*/Franck-Condon factor calculations should assist assignment, allowing vibrational frequencies in the ionic state to be obtained, and the associated AIE to be determined. The first AIE is important in that it can be used in thermodynamic cycles to determine bond dissociation energies of H_2O_2 and $H_2O_2^+$ (25) and it is needed to calculate energies of reactions in solution in which H_2O_2 is oxidized (26) (e.g. the reaction of H_2O_2 with permanganate ions (27)).

Experimental

The experiments reported here were performed on the Circularly Polarized Beamline (4.2R, Polar) at the Elettra synchrotron radiation source (Trieste). The photoelectron spectrometer used in the experiments was specifically designed to study reactive intermediates with PE and CIS (Constant Ionic State) spectroscopies (28-36). This spectrometer has been modified to allow TPE spectra to be obtained (32,33). In order to record TPE spectra, the photoelectron spectrometer was tuned to detect near-zero energy (threshold) photoelectrons. The detection of threshold electrons was optimized using the $Ar^+(^2P_{3/2},^2P_{1/2}) \leftarrow Ar(^1S_0)$ $(3p^{-1})$ TPE spectrum (37). The spectral resolution obtained, when H_2O_2 TPE spectra were acquired, was typically about 7-9 meV as estimated from the full-width at half maximum of the main $(3p)^{-1}$ $Ar^+(^2P_{3/2}) \leftarrow Ar(^1S_0)$ line. Conventional photoelectron (PE) spectra were also recorded as described in earlier work (34-36), using the same procedures to normalize the spectra for the photon flux and the transmission function of the spectrometer. The first band of water and the $(3p^{-1})$ argon doublet were used to calibrate the ionization energy scale of the H_2O_2 PE spectra.

A normal incidence monochromator (NIM) was used on the Polar beamline with either a gold (13.0-22.0 eV) or aluminium grating (8.0-13.0 eV), where the energies shown in brackets are the photon energy ranges covered in this work. The photon energy scale was calibrated using He $1s^2 \rightarrow 1s^1np^1$ (n=2,3) photoabsorptions (38). These were recorded with both first and second order diffracted radiation. The first band of water (AIE = 12.615 eV) (39) provided a check on the photon energy calibration.

H_2O_2 was obtained in the gas-phase for photoelectron measurements by heating a sample of the complex urea:hydrogen peroxide (UHP, Aldrich 97%). This was thoroughly mixed with pure, dry sand (in a 2:1 sand:UHP ratio by weight) and placed in a sample bulb attached to the inlet system of the spectrometer. The sample was carefully heated using a thermostatically controlled water bath to (301.0 ± 0.5) K and the gaseous H_2O_2 passed into flowing argon which passed over the solid sample on the inlet tube of the spectrometer. The inlet tube was a pyrex tube, whose inner surface had been coated with dry boric acid, which had been passivated by extensive exposure to H_2O_2 vapour (40) prior to the TPE measurements. Care was taken to minimise decomposition of H_2O_2 to H_2O and O_2, but a weak first band of H_2O, which rapidly decreased during the measurements, was always observed in the TPE and PE spectra. The long term stability, efficiency, and purity of the H_2O_2 generation was checked in off-line PE experiments with a HeI (21.22 eV) discharge

lamp source prior to the synchrotron measurements. Under typical conditions when TPE spectra were acquired, partial presures used were $\Delta p(H_2O_2)$ =2.5x10^{-7} mbar, and Δp (Ar)= 0.5x10^{-6} mbar. These partial pressures were measured using an ionization gauge connected to the ionization chamber and are with respect to the background pressure in the ionization chamber (3.0x10^{-7} mbar).

Computational details

Geometry optimization calculations were carried out at the BLYP/6-31G**, B3LYP/6-311++G** and RHF/UCCSD(T*)-F12x/VQZ-F12 levels of theory on the $\tilde{X}^1A$ state of H_2O_2, and the $\tilde{X}^2B_g$ and $\tilde{A}^2A_2$ states of $H_2O_2^+$, followed by harmonic vibrational frequency calculations. The BLYP and B3LYP calculations were performed using GAUSSIAN09 (41), while the explicitly correlated F12x calculations, used MOLPRO (42). With the UCCSD(T*)-F12x methods, x can be a or b, giving F12a and F12b energies respectively. Since geometry optimization on the $\tilde{X}^1A$ state of H_2O_2 and the $\tilde{X}^2B_g$ state of $H_2O_2^+$ using both the F12a and F12b energies were found to give the same geometries and relative energies, geometry optimization and all F12x frequency calculations on the $H_2O_2^+$ $\tilde{A}^2A_2$ were carried out using only the F12a method.

In order to assist ionic-state assignments of the PE spectra, especially the photoelectron bands with no resolvable vibrational structure in the 12.0 -21.0 eV ionization energy region, vertical ionization energies (VIEs) to low-lying cationic states of $H_2O_2^+$ were computed using the IP-EOM-CCSD method, with different AVXZ basis sets (aug-cc-pVXZ, X = T, Q or 5), as implemented in ACESII (43). Computed VIEs were extrapolated to the complete basis set (CBS) limit employing the $1/X^3$ formula (44) with the computed VIE values obtained using the AVQZ and AV5Z basis sets.

As vibrational structure was only observed in the first TPE band of H_2O_2, Franck-Condon factors (FCFs) were only calculated for the first photoelectron band. FCFs were computed between the $\tilde{X}^1A$ state of H_2O_2 and the $\tilde{X}^2B_g$ state of $H_2O_2^+$ within the harmonic oscillator model, using the EZSPECTRUM program (45), which includes allowance for the Duschinsky effects. Computed geometrical parameters, harmonic vibrational frequencies and normal modes of the two electronic states involved, obtained from both B3LYP and F12a calculations were used in these FCF calculations. Since the computed FCFs obtained using

B3LYP and F12a inputs were found to be qualitatively very similar, only the theoretically more advanced F12a results are presented here.

Results and Discussion

The results of the calculations performed in this work on the ground state of H_2O_2 and the low-lying cationic states, obtained on one-electron ionization, are shown in Tables 1-3. In Table 1, computed geometrical parameters of the ground state of H_2O_2 and the lowest two electronic states of $H_2O_2^+$ are listed, as well as the corresponding computed H_2O_2 AIE and VIE ionization energies. The ground state of H_2O_2 is computed to have a C_2 structure with a HOOH dihedral angle close to 120°, whereas the ground state and first excited state of $H_2O_2^+$ are computed to have a trans C_{2h} planar geometry and a cis C_{2v} planar geometry respectively (see Figure 1). For the first ionization, because of the large change in equilibrium geometry on ionization, notably the computed HOOH dihedral angle changes from 112.6° to 180°, and the computed O-O bond length decreases from 1.4506 Å to 1.3112 Å (UCCSD(T)-F12b/VQZ-F12 values), there is a significant difference (1.09 eV) between the computed AIE and VIE values (10.66 and 11.75 eV; see Table 1). Similarly, for the second ionization, where again a large change in dihedral angle (from 112.6° to 0.0°) and O-O bond length (1.4506 Å to 1.3093 Å) occurs (the values quoted are UCCSD(T)-F12b/VQZ-F12 values), the difference between the computed AIE and VIE is large (1.78 eV; computed AIE and VIE 11.00 and 12.78 eV). In Table 2, computed harmonic frequencies (in cm^{-1}) are listed for these states of H_2O_2 and $H_2O_2^+$. Experimental fundamental frequencies are only available for the neutral ground state. These show good agreement with the UCCSD(T)-F12b/VQZ-F12 harmonic values (the highest level of theory used in this work to obtain harmonic frequencies) although as expected, because only harmonic values are computed, the UCCSD(T)-F12b/VQZ-F12 values are, in all cases, slightly higher than the experimental fundamental values.

In Table 3, comparison is made between the computed VIEs to the five lowest cationic states, obtained by the IP-EOM-CCSD method with different basis sets, with experimental values obtained from the photoelectron spectrum recorded in this work at a photon energy of 21.22 eV. As can be seen, the agreement between the computed (CBS) and experimental PES values is very good; for example, the CBS first two VIEs are (11.70 ± 0.04) and (12.76 ± 0.04) eV compared with experimental VIEs of (11.74 ± 0.01) and (12.66 ± 0.01) eV. VIEs

obtained by PES have been used in this comparison, rather than TPES VIEs, because whilst observed relative intensities of vibrational components in a PE band in a conventional PE spectrum are almost always governed by Franck-Condon factors between the initial and final ionic state, those observed by TPES may have contributions from autoionization which may lead to non-Franck Condon distributions (46,47).

The PE and TPE spectra recorded in this work are shown in Figures 2-6. As can be seen from these spectra, only the first band shows vibrational structure on its low ionization energy side. This structure is observed with reasonably good resolution in the TPE spectrum (Figures 4 and 5). It is barely seen in the PE spectrum shown in Figures 2 and 3, and in the PE spectra shown in the earlier work of Ashmore and Burgess (19) and Brown (20). As the first band in the TPE spectrum is much better resolved than the first band in the PE spectrum, only the structure in the first band of the TPE spectrum is discussed in this work. Structure is seen in the first band of the TPE spectrum in the 10.5-11.4 eV photon energy region. No resolvable structure is clearly observed above 11.4 eV, probably because of congestion of structure from the first band and weak contributions from the second band (expected AIE 11.0 eV, VIE 12.78 eV; see Table 1). As already stated, the first band of H_2O_2 consists of ionization from a C_2 neutral structure to a trans planar C_{2h} ionic structure. In this ionic state, the torsional potential is reasonably deep as scanning the dihedral angle, θ, with full optimization of the other parameters, at the B3LYP/6-311++G** level, showed that the total energy change from θ = 180 to 90° is significant (1.45 eV at the B3LYP/6-311G** level). In the neutral, the trans and cis barriers are well established as (387.07 ± 0.20) and (2562.8 ± 60.0) cm^{-1} (14). Spectroscopic studies have shown that there are only two torsional vibrational levels, separated by 11.4 cm^{-1}, below the trans barrier, with the next two torsional levels above the barrier, at 254 and 371 cm^{-1} above the lowest level (14). As in the present work ionization is expected to occur from vibrationally equilibrated H_2O_2 at a Boltzmann temperature of 301 K, ionization from all four of these levels should be taken into account. (The next two torsional levels are at 567 and 776 cm^{-1} (14) and are not expected to be significantly populated under the conditions of the experiment).

Franck-Condon factor (FCF) simulations of the vibrational structure of the first photoelectron band of H_2O_2 were carried out using the UCCSD(T)-F12a/cc-pVQZ-F12 computed equilibrium geometries and vibrational frequencies of the ground electronic states of H_2O_2 and $H_2O_2^+$ shown in Tables 1 and 2. As the ground state of the neutral is a C_2 structure and that of the ion is a trans structure of C_{2h} symmetry, the common symmetry

elements are those of a C_2 point group. H_2O_2 has six vibrational modes and in C_2 symmetry four are of ***a*** symmetry (a O-H symmetric stretch (ω_1), a O-H symmetric bend (ω_2), a O-O stretch (ω_3) and a HOOH torsion mode (ω_4)) and are expected to be excited in single quanta excitations on ionization from the ground state of the neutral. The other two modes are of ***b*** symmetry. The FCF simulations show that the main structure observed on the leading edge of the first photoelectron band (in the ionization energy region 10.5-11.4 eV) is in the O-O stretching mode (ω_3) and the HOOH deformation mode (ω_4). This is consistent with the main change in equilibrium geometry being in the O-O bond length, which decreases, and the HOOH dihedral angle, which increases, upon ionization.

In the ion, the harmonic oscillator model is expected to be adequate, to achieve assignment of the vibrational structure, as the potentials for the O-O stretch and HOOH torsion modes are expected to have significant depth; the O-O bond dissociation energy in $H_2O_2^+$ can be estimated as 4.5 eV (from the known O-O bond dissociation energy of H_2O_2 eV (48) and the available AIEs of OH and H_2O_2; see later text) , and for the HOOH torsion mode, as already stated, the total energy change from θ = 180° to 90° is significant (1.45 eV at the B3LYP level). In the neutral, the harmonic oscillator model is expected to be appropriate for ω_3 but not for ω_4 because of the double minimum potential in the torsional mode. However, the UCCSD(T)-F12a/cc-pVQZ-F12 computed vibrational wavenumber of 381.9 cm^{-1} is expected to be adequate to generate the wavefunction of the lowest vibrational level of the torsion mode, which is below the trans barrier, but inadequate for the torsional vibrational levels above the barrier, notably the torsional levels at 254 and 371 cm^{-1} (14) above the lowest torsional level. These two levels are expected to be populated at 300 K. Simulations were therefore carried out at Boltzmann vibrational temperatures of 0 and 300 K, but with only the lowest vibrational level in the torsion mode populated i.e. no “hot band” ionizations were considered in the torsional mode, although they are included in other modes. The main components in the experimental spectrum in the 10.5-11.0 eV ionization energy region are labelled as **a**, **a′** and **a″**, **b**, **b′**, and **b″**, and **c** in Figure 6.

Two ways of aligning the simulated spectrum with the experimental spectrum were considered. These involved:

(a) Aligning the two most intense features in the 10.75-10.82 eV region in the simulation with features **b** and **a′** in the experimental spectrum. This involves a shift of the simulated spectrum of -0.011 eV.

(b) Aligning the most intense feature in the 10.75-10.82 eV region in the simulation with feature **a′** in the experimental spectrum, and assuming that **b** is a hot-band of **a′** in the torsional mode. This would be consistent with the **b-a′** separation. It involves a +0.025 eV shift of the simulated spectrum. These two possibilities are now considered:

(a) A -0.011 eV shift of the simulated spectrum.

This possibility arose because comparison of the 300K simulated spectrum with the experimental spectrum indicated that the components **b** and **a′** could line up with the intense components in the simulation in the 10.75-10.82 eV region. This would mean moving the AIE component down from 10.660 eV (the AIE value used in the simulation which is the best computed value, see Table 1) to 10.649 eV, the experimental position of **a**, by -0.011 eV. With this alignment, the **a-b** separation is (900 ± 20) cm^{-1} and the **a-a′** separation is (1110 ± 20) cm^{-1}, and the simulation indicates that these separations are excitation respectively of one quantum in ω_4 and one quantum in ω_3 in the ion (computed UCCSD(T)-F12a/VQZ-F12 values 880 and 1211 cm^{-1}). With this assignment, **a** is the adiabatic component, **b** is excitation of ω_4 , **a′** is excitation of ω_3, **a″** is excitation of $2\omega_3$, **b′**and **b″** are excitation of $2\omega_4$ and $3\omega_4$, and **c** is excitation $\omega_3 + \omega_4$ upon ionization. However, above band **c** (10.895 eV), the agreement between the computed band positions and intensities, and the experimental spectrum becomes very poor. Also, the excited torsional vibrational levels (at 254 and 371 cm^{-1} (14)) are expected to be populated at 300 K. Their populations at this temperature relative to the lowest vibrational level are calculated as 0.30 and 0.17 assuming a Boltzmann distribution. As these two torsional vibrational levels are above the trans-barrier in the neutral ground state, ionizations from these levels are expected to have significant Franck-Condon factors to torsional levels with low vibrational quantum numbers in the ion, much larger than from the two almost degenerate levels below the barrier. With this assignment, for the -0.011 eV shift shown in Figure 7, there are no clearly resolved features to the low photon energy side of each "main peak", displaced by 0.031 eV (254 cm^{-1}) and 0.046 eV (371 cm^{-1}) to low photon energy, which could be assigned to "hot bands" arising from ionizations from these levels. Therefore, this assignment shown in Figure 7, with a -0.011 eV displacement is discounted.

(b) A +0.025 eV shift of the simulated spectrum.

This possibility was considered because the simulated spectrum with the +0.025 eV shift, showed reasonably good agreement with the experimental spectrum in the 10.9-11.4 eV region (see Figure 8) and because of the expected large Franck-Condon factors for ionization

from the third and fourth torsional vibrational levels in the neutral (at 254 and 371 cm^{-1}) to torsional levels with low vibrational quantum numbers in the ion (they are effectively planar-to-planar ionizations). Contributions from ionizations from these levels (i.e. "hot bands") to the experimental spectra were considered. In particular, the possibility was investigated that **b** is a "hot band" associated with **a′** as the separation of their band maxima (0.026 ±0.003 eV) is close to that expected for the 254 cm^{-1} separation in the neutral (0.031 eV). To allow this assignment, the computed AIE of 10.660 eV would have to be moved by +0.025 eV to 10.685 eV. The simulation with this displacement (Figure 8) shows that all features up to 11.0 eV can be assigned and the agreement of the main bands, in terms of intensity and position in the 10.5-11.4 eV photon energy region, in the experimental spectrum with those in the simulated spectrum is reasonably good. This assignment means that the adiabatic component (at 10.685 eV) is expected to have 'hot-band' contributions at 10.654 and 10.639 eV, for ionization from the 254 and 371 cm^{-1} levels in the neutral to the ground vibrational state of the ion. These values agree, within experimental error, with the measured position of band **a** (at 10.649 eV) and the measured position of the feature to low IE of band **a** (at 10.635 eV). This assignment means that the adiabatic component is not observed directly, but is obtained from the aligning of the higher bands, notably bands **a′** and **c** , to the experimental bands. With this assignment, **a′** arises from excitation of one quantum of ω_4, **c** arises from excitation of two quanta of ω_4 and **b″** arises from excitation of one quantum of ω_4 and one quantum of ω_3 in the ion. Then **b** is a hot-band associated with **a′**, **b′** is a hot-band associated with **c,** and **a″** is a hot band associated with **b″**. **a** and the feature on its low energy side are hot bands associated with the adiabatic component, where all these hot bands arise from excitation of torsional modes in the neutral. With this assignment, using the experimental position of **c** and **b″** with the AIE of 10.685 eV gives ω_4 = (850 ± 30) cm^{-1} and ω_3 = (1340 ± 30) cm^{-1}. These values compare reasonably well with the UCCSD(T)-F12/cc-pVQZ-F12 values of ω_4 and ω_3 in the ion 880 and 1211 cm^{-1} . It should be emphasized that the simulated spectrum shown in Figure 8 does not include hot-bands in the torsional mode. Features which are associated with these hot-bands, marked with a '*' in this figure, are identified on the basis that their separation from an assigned band, for ionization from the lowest vibrational level in the neutral, is consistent with the known torsional vibrational energy separation in the neutral. Clearly, support for these assignments must await improved Franck-Condon factor calculations which involve calculation of accurate vibrational wavefunctions for the torsional levels in the neutral both below and above the trans barrier, and calculation of Franck-

Condon factors for ionization from these levels to vibrational levels in the ion. An anharmonic method must also be used for the other modes rather than the harmonic method used here. A simplification of the experimental spectrum is planned by generating internally cold H_2O_2 in a molecular beam and recording a higher resolution TPE spectrum. Significant cooling of the sample in this way might remove the major part, or even all, of the hot-band spectral contributions. Nevertheless, the method used here is thought to be sufficient to assign the observed structure and determine an improved AIE of H_2O_2.

The first AIE obtained in this work, 10.685 ± 0.005 eV, from the preferred assignment of the structure observed in the 10.5-11.5 eV photon energy region of the TPE spectrum of the first band of H_2O_2 compares with previously reported values of (10.62 ± 0.02) eV (16) and (10.54 ± 0.02) eV (20) by conventional photoelectron spectroscopy, (10.92 ± 0.05) eV measured by electron impact mass spectrometry (21), and (10.631 ± 0.007) eV determined by photoionization mass spectrometry (PIMS) (22). Two values have also been derived from electronic structure calculations, 10.36 eV by SD-CI calculations (23) and 10.57 eV by CCSD(T) calculations (49); these compare with the value of 10.660 eV recommended in this present work from UCCSD(T)-F12/VQZ-F12 calculations. All of the experimental values, including the value in the present work, were obtained from an effusive vapor source at, or close to, room temperature, and, as discussed, they are all expected to have contributions from ionization of vibrationally excited levels, notably from the excited torsional levels above the trans-barrier at 254 and 371 cm^{-1} above the lowest neutral vibrational level (14). The most precise value (10.631 ± 0.007) eV, derived from the PIMS study, was obtained by selecting the point of half-height in the first step recorded in the $H_2O_2^+$ photoion yield vs photon energy curve (a photoionization efficiency (PIE) curve). However, it is clear that this PIE curve must be affected by ionization from vibrationally excited levels in the neutral, and it is notable that 10.631 eV corresponds, within experimental error, to the band on the low IE side of band **a**, (measured in this work as 10.635 eV) which corresponds, in the assignment proposed, to ionization from the 371 cm^{-1} level of the neutral to the lowest vibrational level in the ion. (10.685 ± 0.005) eV, the recommended value in this work, corresponds to the top of the first step of the PIE curve recorded in the PIMS study (22).

The first AIE of H_2O_2 derived in this work has implications for the heat of formation of $H_2O_2^+$, and the bond dissociation energies of $H_2O_2^+$ notably D(HO-OH^+) and D(H-O_2H^+). The heat of formation of $H_2O_2^+$ can be derived from

$$AIE\ (H_2O_2) = \Delta H_{f,298}\ (H_2O_2^+) - \Delta H_{f,298}\ (H_2O_2) \qquad (4)$$

Using the heat of formation of H_2O_2, $\Delta H_{f,298}$ (H_2O_2) – (32.48 ± 0.05) kcal.mol^{-1} (50), with the new AIE of H_2O_2 yields $\Delta H_{f,298}$ ($H_2O_2^+$) = (213.9 ± 0.2) kcal.mol^{-1} , which compares with (212.7 ± 0.2) kcal.mol^{-1} determined by Litorja and Ruscic by PIMS (22).

The bond dissociation energies of $H_2O_2^+$ can be related to other thermodynamic quantities in the following way:

$$D(HO\text{-}OH^+) = D(HO\text{-}OH) + AIE(OH) - AIE(H_2O_2) \quad (5)$$

$$D(H\text{-}O_2H^+) = D(H\text{-}O_2H) + AIE(HO_2) - AIE(H_2O_2) \quad (6)$$

Taking $D_{0,298}$ (HO-OH) = (50.26 ± 0.23) kcal.mol^{-1} and $D_{0,298}$ (H-O_2H) as (87.9 ± 0.8) kcal.mol^{-1} (50, and Supplementary Information, SI), with AIE(OH) = (13.0170 ± 0.0002) eV (51,52) and AIE(HO_2) = (11.35 ± 0.01)eV (53) gives $D_{0,298}$ (HO-OH^+) and $D_{0,298}$ (H-O_2H^+) as (104.0 ± 1.3) and (103.2 ± 1.0) kcal.mol^{-1} respectively which compare with the values that can be derived from the PIMS work of Litorja and Ruscic (22) of (106.32 ± 0.17) and (104.5 ± 1.1) kcal.mol^{-1}. It is interesting that $D_{0,298}$ (HO-OH^+) > $D_{0,298}$ (H-O_2H^+), although they are very close (within 2.0 kcal.mol^{-1}), whereas for the corresponding neutral dissociation energies the order is reversed, $D_{0,298}$ (HO-OH) < $D_{0,298}$ (H-O_2H), with the difference being much larger (~ 37 kcal.mol^{-1}).

Conclusions

H_2O_2 has been studied by TPE and PE spectroscopy. Five bands have been observed in the 10.0-21.0 eV ionization energy region which have been assigned by high level electronic structure calculations.

Vibrational structure has only been resolved in the first TPE band, on its leading edge in the 10.5-11.4 eV ionization energy region. Comparison of this structured spectrum with a simulated spectrum computed using harmonic Franck Condon factors shows that this structure is in the O-O stretching mode (ω_3) and the HOOH deformation mode (ω_4). This gives the first AIE of H_2O_2 as (10.685 ± 0.005) eV, and ω_4 = (850 ± 30) and ω_3 =(1340 ±30) cm^{-1} in the $\tilde{X}^2B_g$ state of $H_2O_2^+$. Contributions from ionization of vibrationally excited levels in the torsion mode in neutral H_2O_2 have been identified in this structured spectrum.

This work has demonstrated the need for a well resolved TPE spectrum of H_2O_2 which has been sufficiently cooled that hot-bands from ionization of excited torsional levels do not appear in the spectrum. It has also highlighted the need for reliable Franck-Condon factors for the first photoelectron band which have been derived from a potential which describes the double minimum potential in the neutral ground state accurately. It is hoped that this work will stimulate experimental and theoretical interest in this problem to test the assignments presented and the derived AIE.

Acknowledgements

The authors are grateful to NERC for supporting the experimental work and to the EPSRC National Service for Computational Chemistry (NSCCS) for the provision of computational resources. L. S. thanks the CNR-IOM Institute for financial support under the EUROFEL Design Study Project. V. Z. acknowledges the Swedish Research Council (VR) for financial support. We also thank Drs S. Tuchini, N. Zema, and D. Catone of the Polar beamline (4.2R) at Elettra (Trieste) for help and advice. Support from the Research Grants Council of the Hong Kong Special Administrative Region is also acknowledged (under grant refs GRF PolyU 5011/12P and PolyU 153013/15P).

.

Table 1. Computed geometrical parameters (bond lengths in Å and angles in degrees) of the $\tilde{X}^1A$ state of H_2O_2, the $\tilde{X}^2B_g$ and $\tilde{A}^2A_2$ states of $H_2O_2^+$ and their ionization energies (AIE_e and VIE in eV) obtained at different levels of theory.

$\tilde{X}^1A$ (C_2) **neutral H_2O_2**	**OH/Å**	**OO/Å**	**HOO/°**	**HOOH/°**	**AIE_e/eV**	**VIE/eV**
BLYP/6-31G**	0.9825	1.4944	98.54	120.06		
B3LYP/6-311++G**	0.9672	1.4540	100.47	121.19		
UCCSD(T*)-F12a/VQZ-F12[a]	0.9634	1.4506	100.10	112.68		
UCCSD(T*)-F12b/VQZ-F12[a]	0.9634	1.4506	100.10	112.67		
IR[b]	0.95	1.475	94.8	119.8		
MP2(fu)/6-31G* in G2[c]	0.976	1.468	98.7	121.2		
B3LYP/6-311+G(3df,2p)[c]	0.966	1.446	100.9	112.0		
$\tilde{X}^2B_g$ (C_{2h}) **trans- $H_2O_2^+$**						
BLYP/6-31G**	1.0124	1.3517	103.03	180.0	9.87	10.76
B3LYP/6-311++G**	0.9972	1.3092	104.82	180.0	10.59	11.57
IP_EOM:CCSD/AVTZ[d]						11.52
IP_EOM:CCSD/AVQZ[d]						11.62
IP_EOM:CCSD/AV5Z[d]						11.66
IP_EOM:CCSD/CBS[d]						11.70
UCCSD(T*)-F12a/VQZ-F12[a]	0.9919	1.3113	103.79	180.0	10.64	11.75
UCCSD(T*)-F12b/VQZ-F12[a]	0.9918	1.3112	103.79	180.0	10.63	11.74
Average (F12a/F12b)					10.64	11.75
Best AIE_0					10.66	
PES[e]					10.62 (10.54)	11.70 (11.51)
PIMS[c]					10.631±0.007	
G2[c]	1.007	1.351	-	180.0	10.71	
B3LYP/6311+G(3df,2p)[c]	0.995	1.307	-	180.0	10.56	
TPES[f]					10.685±0.005	
PES [f]						11.74
$\tilde{A}^2A_2$ (C_{2v}) **cis-$H_2O_2^+$**[, g]						
BLYP/6-31G**	1.0124	1.3475	110.74	0.0	10.27	[h]
B3LYP/6-311++G**	0.9973	1.3065	111.98	0.0	11.00	12.94
IP_EOM:CCSD/AVTZ[d]						12.59

IP_EOM:CCSD/AVQZ[d]						12.69
IP_EOM:CCSD/AV5Z[d]						12.72
IP_EOM:CCSD/CBS[d]						12.76
UCCSD(T*)-F12a/VQZ-F12	0.9917	1.3093	111.46	0.0	10.99	12.80
UCCSD(T*)-F12b/VQZ-F12[i]					10.98	12.78
Average (F12a/F12b)					10.99	12.79
Best AIE_0					11.00	

[a] The computed relative F12a and F12b energies are the same at both F12a and F12b optimized geometries.
[b] Ref. (13)
[c] Photoionization mass spectrometry and ab initio/DFT calculations; ref. (22)
[d] VIE's were computed using IP-EOM CCSD single geometry calculations, as installed in ACESII, at the optimized UCCSD(T*)-F12a/VQZ-F12 geometry of neutral H_2O_2; CBS refers to extrapolation of the AVQZ and AV5Z VIE values to the complete basis set limit employing the $1/X^3$ formula (ref. (44)).
[e] Photoelectron spectrum; ref. (19); values from ref. (20) in brackets.
[f] Present study.
[g] The 1^2A_2 state of cis-$H_2O_2^+$ is the lowest state at its optimized geometry (*i.e.* the lowest state with the cis structure).
[h] The $1\ ^2A$ state converged to the $\tilde{X}\ ^2B$ state at the neutral C_2 optimized geometry.
[i] At F12a optimized geometries.

Table 2. Computed harmonic vibrational frequencies (ω_n) and experimental fundamental (ν_n) vibrational frequencies (in cm^{-1}) of the $\tilde{X}\,^1A$ state of H_2O_2 and the $\tilde{X}\,^2B_g$ and $\tilde{A}\,^2A_2$ states of $H_2O_2^+$ obtained by different methods.

$\tilde{X}^1A$ (C_2) **H_2O_2**	a				b	
	ω_1/ν_1	ω_2/ν_2	ω_3/ν_3	ω_4/ν_4	ω_5/ν_5	ω_6/ν_6
	s-OH	s-bend	OO	torsion	a-OH	a-bend
BLYP/6-31G**	3599.6	1378.4	868.9	321.4	3600.9	1241.0
B3LYP/6-311++G**	3779.3	1453.2	934.3	365.3	3778.4	1296.2
UCCSD(T)-F12a/VQZ-F12	3797.4	1437.0	911.8	381.9	3797.3	1329.2
IR/Raman (lowest)[a]	3593	1385	866	255	3560	1265
IR/Raman (highest)[a]	3618	1394	878	378	3619	1294
HF/6-31G* (scaled)[b]	3653	1460	1028	356	3655	1333
B3LYP/6-311+G(3df,2p)[b]	3704	1416	933	387	3704	1310
$\tilde{X}^2B_g$ (C_{2h}) **trans-$H_2O_2^+$**	a_g			a_u	b_u	
BLYP/6-31G**	3303.8	1540.3	1118.6	832.6	3284.0	1262.3
B3LYP/6-311++G**	3444.8	1587.1	1241.2	872.0	3421.5	1301.2
UCCSD(T)-F12a/VQZ-F12	3501.9	1600.9	1211.5	880.0	3483.3	1322.6
HF/6-31G* (scaled)[b]	3337	1557	1395	867	3295	1282
B3LYP/6-311+G(3df,2p)[b]	3385	1570	1229	851	3365	1295
PES [c]			1050 (1080)			
TPES[d]			1340 ±30	850±30		
$\tilde{A}^2A_2$ (C_{2v}) **cis-$H_2O_2^+$**	a_1			a_2	b_2	
BLYP/6-31G**	3304.3	1337.7	1101.6	647.2	3242.2	1433.2
B3LYP/6-311++G**	3447.5	1365.8	1228.0	670.9	3385.5	1473.5
UCCSD(T)-F12a/VQZ-F12	3495.8	1407.0	1200.9	717.7	3469.8	1532.3

[a] From the compilation in ref. (54) both in gas phase and various inert gas matrices.

[b] Scaled HF (by 0.8929 in G2) and B3LYP vibrational frequencies from ref. (22)

[c] Ref. (19); values from ref. (20) in brackets

[d] this work

Table 3. Computed vertical ionization energies (in eV) of H_2O_2 to five lowest-lying cationic states obtained by the IP_EOM CCSD method with different basis sets.

$H_2O_2^+$ states	AVTZ	AVQZ	AV5Z	CBS (1/X^3:AVQZ;AV5Z)	PES This work	PES ref. (19)
1^2B	11.520	11.620	11.660	11.70±0.04	11.74 ± 0.01	11.7
1^2A	12.592	12.688	12.725	12.76±0.04	12.66 ± 0.01	13.0
2^2A	15.434	15.520	15.554	15.59±0.04	15.36 ± 0.01	15.4
2^2B	17.464	17.545	17.576	17.60±0.03	17.45 ± 0.02	17.5
3^2A	18.644	18.719	18.747	18.77±0.03	18.20± 0.05	18.5

Captions to figures

Figure 1. Optimized structures of the ground state of H_2O_2 and the lowest two states of $H_2O_2^+$ (see text and Table 1).

Figure 2. Computed vertical IEs by the IP-EOM CCSD method with basis set extrapolation to the CBS limit, compared with the experimental HeI PE spectrum. (The spectrum contains contributions from the HeIα, HeIβ and HeIγ $(3p)^{-1}$ $Ar^+(^2P) \leftarrow Ar(^1S_0)$ ionizations; these are the three sets of sharp doublet features at ~ 15.8, ~ 14.0, and ~ 13.3 eV).

Figure 3
HeI (21.22 eV) PE spectrum of H_2O_2 in the 10.0-14.0 eV IE region

Figure 4
TPE spectrum of H_2O_2 recorded in the 10.0-20.0 eV photon energy region.

Figure 5
TPE spectrum of H_2O_2 recorded in the 10.0-14.0 eV photon energy region.

Figure 6
TPE spectrum of H_2O_2 recorded in the 10.5-12.0 eV photon energy region, showing the main resolved features in the 10.5-11.0 eV region (a, a′, a″, b, b′, b″, c).

Figure 7
Comparison of the experimental TPE spectrum of H_2O_2 in the 10.5-11.4 eV photon energy region with the simulated 300 K spectrum, with no 'hot-bands' from the torsional mode in the simulation. The simulated spectrum has been shifted by -0.011 eV (AIE = 10.660-0.011 = 10.649 eV; see text). Each component is simulated with a gaussian of 30 meV half-width.

Figure 8
Comparison of the experimental TPE spectrum of H_2O_2 in the 10.5-11.4 eV photon energy region with the simulated 300 K spectrum, with no 'hot-bands' from the torsional mode in the simulation. The simulated spectrum has been shifted by +0.025 eV (AIE = 10.660+0.025 = 10.685 eV; see text). Each component is simulated with a gaussian of 30 meV half-width. The assignment of bands a, a′, a″, b, b′,b″ and c is shown in this Figure and given in the text. With this assignment, bands d and e shown in Figure 6 correspond to excitation of $3\omega_3$, $\omega_3+3\omega_4$ (d) and $4\omega_3$, $2\omega_3+3\omega_4$ (e) in the ion.

References

(1) Finlayson-Pitts, B. J.; Pitts, J. N. *Chemistry of the Upper and Lower Atmosphere*; Academic Press: San Diego 2000.

(2) Zabaikin, V. A.; Perkov, E. V.; Tretyakov, P. K. Effect of an H_2O_2 additive on hydrogen ignition and combustion in a supersonic air flow. *Combustion, Explosion and Shock Waves* **1997**, *33*, 301-305.

(3) El-Asrag, H. A.; Ju, Y. Direct numerical simulations of exhaust gas recirculation effect on multistage autoignition in the negative temperature combustion regime for stratified HCCl flow conditions by using H_2O_2 addition. *Combust. Theory Model.* **2013**, *17*, 316-334.

(4) Cooper, M. S.; Heaney, H.; Newbold, A. J.; Sanderson, W. R. Oxidation reactions using urea-hydrogen peroxide: a safe alternative to anhydrous hydrogen peroxide. *Synlett* **1990**, no 9, 533-535.

(5) Beckman, K. B.; Ames, B. N. The free radical theory of aging matures. *Physiol. Rev.* **1998**, *78*, 547-581.

(6) Rizzo T. R.; Hayden, C. C.; Crim, F. F. State-resolved product detection in the overtone vibration initiated unimolecular decomposition of HOOH ($6\nu_{OH}$). *J. Chem. Phys.* **1984**, *81*, 4501-4509.

(7) Dubai, H. R.; Crim, F. F. Vibrational overtone predissociation spectroscopy of hydrogen peroxide. *J. Chem. Phys.* **1985,** *83*, 3863-3812.

(8) Klee, S.; Gericke, K. H.; Comes, F. J. Photodissociation of H_2O_2, D_2O_2 from the lowest excited state--the origin of fragment rotation. *Ber Bunsenges Phys. Chem.* **1988**, *92*, 429-434.

(9) Powis I., The influence of vibrational parity in chiral photoionization dynamics. *J. Chem. Phys.* **2014**, *140*, 111103.

(10) Lombardi, A.; Palazzetti, F.; Maciel G. S.; Aquilanti, V.; Sevryuk, M. B. Simulation of oriented collision dynamics of simple chiral molecules, *Int. J. Quant. Chem.* **2011,** *111*, 1651-1658.

(11) Barreto, P. R. P.; Vilela, A. F. A.; Lombardi, A.; Maciel, G. S., Palazzetti, F., Aquilanti, V. The hydrogen peroxide-rare gas systems: quantum chemical calculations and hyperspherical harmonic representation of the potential energy surface for atom-floppy molecule interactions. *J. Phys. Chem. A* **2007**, *111*, 12754-12762.

(12) Walker, R. W.; Morley, C. Basic Chemistry of Combustion, Comprehensive Chemical Kinetics, Low-Temperature Combust and Autoignition. **1997**, *35*, 1-124.

(13) Redington, R. L.; Olson, W. B.; Cross, P. C. Studies of hydrogen peroxide: The infrared spectrum and the internal rotation problem. *J. Chem. Phys.* **1962,** *36*, 1311-1326.

(14) Flaud, J. M.; Camy-Peyet, C.; Johns, J. W. C.; Carli, B. The far infrared spectrum of H_2O_2: First observation of the staggering of levels and determination of the cis barrier. *J. Chem. Phys.* **1989**, *91*, 1504-1510.

(15) Hunt, R. H.; Leacock, R. A.; Peters, C. W.; Hecht, K. T. Internal rotation in hydrogen peroxide; the far-infrared spectrum and the determination of the hindering potential. *J. Chem. Phys.* **1965**, *42*, 1031-1946.

(16) Cook, W. B.; Hunt, R. H.; Shelton, W. N.; Flaherty, F. A. Torsion-rotation energy levels, hindered potential and inertial parameters for the first excited vibrational state of the antisymmetric O-H stretch in hydrogen peroxide. *J. Mol. Spec.* **1995**, *171*, 91-112.

(17) Petkie, D. T.; Goyette, T. M.; Holton, J. J.; de Lucia, F. C.; Helminger, P. Millimetre/submillimetre–wave spectrum of the first excited torsional state in HOOH. *J. Mol. Spec.* **1995**, *171*, 145-159.

(18) Osafune, K.; Kimura, K. Photoelectron spectroscopic study of hydrogen peroxide. *Chem. Phys. Letts.* **1974**, *25*, 47-50.

(19) Ashmore, F. S.; Burgess, A. R. Study of some medium size alcohols and hydroperoxides by photoelectron spectroscopy. *J.C.S. Faraday II* **1977**, *73*, 1247-1261.

(20) Brown, R. S. A photoelectron investigation of the peroxide bond. *Can. J. Chem.* **1975,** *53*, 3439-3447.

(21) Foner, S. N.; Hudson R. L. Ionization and dissociation of hydrogen peroxide by electron impact. *J. Chem. Phys.* **1962**, *36*, 2676-2680.

(22) Litorja, M.; Ruscic B. A photoionization study of the hydroperoxy radical, HO_2, and hydrogen peroxide, H_2O_2. *J. Electron Spectrosc. Relat. Phenom.* **1998**, *97*, 131-146.

(23). Takeshita, K.; Mukherjee, P. K. Theoretical study on the first band of the photoelectron spectrum of H_2O_2 with inclusion of vibrational structure. *Chem. Phys. Letts*. **1989**, *160*, 193-199.

(24) Camy-Peyret, C.; Flaud, J. M.; Johns, J. W. C.; Noel, M. Torsion-vibration interaction in H_2O_2: first high resolution observation of ν_3. *J. Mol. Spec.* **1992,** *155*, 84-104.

(25) Dyke, J. M. Photoionization of reactive intermediates of importance in the atmosphere" in Chemistry for Sustainable Development **2012**, 34-56 Gupta Bhowon M., Jhaumeer-Laulloo S., Li Kam Wah H. and Ramasami P. (Eds) Springer (Berlin).

(26) Morrison, M. M.; Roberts, J. L.; Sawyer, D. T. Oxidation-reduction chemistry of hydrogen peroxide in aprotic and aqueous solutions. *Inorg. Chem.* **1979**, *18*, 1971-1973.

(27) Bowman, M. I. The reaction between potassium permanganate and hydrogen peroxide *J. Chem. Ed.* **1949**, *26*, 103-104.

(28) Beeching, L. J.; Dias, A. A.; Dyke, J. M.; Morris, A.; Stranges, S.; West, J. B.; Zema N.; Zuin, L. Photoelectron spectroscopy of atomic oxygen using the Elettra synchrotron source. *Mol. Phys.* **2003**, *101*, 575-582.

(29) Innocenti, F.; Zuin, L.; Costa, M. L.; Dias, A. A.; Morris, A.; Paiva, A. C. S.; Stranges, S.; West, J. B.; Dyke, J. M. Photoionization studies of atmospherically important species N and OH at the Elettra synchrotron radiation source. *J. Electron Spectrosc. Relat. Phenom.* **2005**, *142*, 241-252.

(30). Zuin, L.; Innocenti. F.; Costa, M. L.; Dias, A. A.; Morris, A.; Paiva, A. C. S.; Stranges, S.; West, J. B,; Dyke, J. M. An initial investigation of S and SH with angle resolved photoelectron spectroscopy using synchrotron radiation. *Chem. Phys.* **2004**, *298*, 213-222.

(31) Innocenti F., Zuin, L.; Costa, M. L.; Dias, A. A.; Morris, A.; Stranges, S.; Dyke, J. M. Measurement of the partial photoionization cross sections and asymmetry parameters of S atoms in the photon Energy range 10.0-30.0 eV using constant-ionic-state spectroscopy. *J. Chem. Phys.* **2007**, *126*, 154310.

(32) Innocenti, F.; Eypper, M.; Beccaceci, S;, Morris. A.; Stranges, S.; West, J. B.; King, G. C., Dyke, J. M. A study of the reactive Intermediate IF and I Atoms with Photoelectron Spectroscopy. *J. Phys. Chem. A* **2008**, *112*, 6939-6949.

(33) Innocenti, F.; Eypper, M.; Lee, E. P. F.; Stranges, S.; Mok, D. K. W.; Chau, F. T.; King,

G. C.; Dyke, J. M. Difluorocarbene Studied by Threshold Photoelectron Spectroscopy (TPES): Measurements of the First Adiabatic Ionization Energy (AIE) of CF_2. *Chem.-Eur. J.* **2008**, *14*, 11452-11460.

(34) Dyke, J. M.; Haggerston, D.; Morris, A.; Stranges, S.; West, J. B.; Wright, T. G.; Wright, A. E., A study of the SO molecule with photoelectron spectroscopy using synchrotron radiation. *J. Chem. Phys.* **1997**, *106*, 821-830.

(35) Dyke, J. M.; Gamblin, S. D.; Morris, A.; Wright, T. G.; Wright, A. E.; West J. B. A photoelectron spectrometer for studying reactive intermediates using synchrotron radiation, *J. Electron Spectrosc. Relat. Phenom.* **1998**, *97*, 5-14.

(36) West, J. B.; Dyke, J. M.,; Morris, A.; Wright, T. G.; Gamblin, S. D. Photoelectron spectroscopy of short-lived molecules using synchrotron radiation. *J. Phys. B: At. Mol. Opt. Phys.* **1999**, *32*, 2763–2782.

(37) Hall, R. I.; McConkey, A.; Ellis, K.; Dawber, G.; Avaldi, L.; MacDonald, M. A.; King, G. C. A penetrating field electron-ion coincidence spectrometer for use in photoionization studies. *Meas. Sci. Technol.* **1992**, *3*, 316-324.

(38) Helium atomic term values in http://physics.nist.gov/cgi-bin/ASD/energy1.pl

(39) Karlsson, L.; Mattsson, L.; Jadrny, R.; Albridge, R. G.; Pinchas, S.; Bergmark, T.; Siegbahn, K. Isotopic and vibronic coupling effects in the valence electron spectra of $H_2{}^{16}O$, $H_2{}^{18}O$, and $D_2{}^{16}O$. *J. Chem. Phys.* **1975**, *62*, 4745-4752.

(40) Baldwin, R. R.; Mayor, L. The mechanism of the hydrogen + oxygen reaction in aged boric-acid-coated vessels, *Trans. Faraday Soc.*, **1960**, *56*, 103-114.

(41) Frisch, M. J.; Trucks, G. W.; Schlegel, H. B.; Scuseria, G. E.; Robb, M. A.; Cheeseman, J. R.; Scalmani, G.; Barone, V.; Mennucci, B.; Petersson, G. A.; *et al.* Gaussian 09, revision A.02; Gaussian, Inc.:Wallingford, CT, **2009**.

(42) Werner, H.-J.; Knowles, P. J.; Knizia, G.; Manby, F. R.; Schutz, M.; *et al.* MOLPRO, version 2010.1, see http://www.molpro.net

(43) ACES II is a program product of the Quantum Theory Project, University of Florida. Authors: Stanton, J. F.; Gauss, J.; Perera, S. A.; Watts, J. D.; Yau, A. D.; Nooijen, M.; Oliphant, N.; Szalay, P. Z.; Lauderdale, W. J.; Gwaltney, S. R.; Beck, S.; Balkov´a, A.; Bernholdt, D. E.; Baeck K. K.; Rozyczko P.; Sekino, H.; Huber, C.; Pittner, J.; Cencek, W.; Taylor, D.; Bartlett, R. J. Integral packages included are VMOL (Almlof, J.; Taylor, P. R.); VPROPS (Taylor, P.;); ABACUS (Helgaker, T.; Jensen, H. J. A.; Jørgensen, P.; Olsen, J.; Taylor, P. R.;); HONDO/GAMESS (Schmidt, M. W.;, Baldridge, K. K.; Boatz, J. A.; Elbert, S. T.; Gordon, M. S.; Jensen, J. J.; Koseki, S.; Matsunaga, N.; Nguyen, K. A.; Su. S.; Windus, T. L.; Dupuis, M.; Montgomery, J. A.;). **2013**

(44) Halkier, A.; Helgaker, T.; Klopper, W.; Jorgensen, P.; Csaszar A. G. Comment on "Geometry Optimization with an Infinite Basis Set" [*J. Phys. Chem. A* **1999**, *103*, 651] and "Basis-set Extrapolation" [*Chem. Phys. Lett.* **1998**, *294*, 45)] *Chem. Phys. Lett*. **1999**, *310*, 385-389.

(45) Mozhayskiy, V.; Krylov, A. eZSpectrum v3.0 http://iopenshell.usc.edu 2009

(46) Guyon, P. M.; Spohr, R.; Chupka, W. A.; Berkowitz J. Threshold photoelectron spectrum of HF, DF and F_2 *J. Chem. Phys.* **1976**, *65*, 1650-1658.

(47) Baer, T.; Guyon, P. M. Autoionization and isotope effect in the threshold photoelectron spectrum of $^{12}CO_2$ and $^{13}CO_2$. *J. Chem. Phys.* **1986**, *85*, 4765-4778.

(48) Bach, R. D.; Ayala, P. Y.; Schlegel, H. B. A re-assessment of the bond dissociation energies of peroxides: an *ab initio* study. *J.A.C.S.* **1996**, *118*, 12758-12765.

(49) Ferreira, C.; Martiniano, H. F. M. C.; Costa Cabral, B. J.; Aquilanti, V. Electronic Excitation and Ionization of hydrogen peroxide water clusters: comparison with water clusters. *Int. J. Quant. Chem.* **2011**, *111*, 1824-1835.

(50) Gurvich, L. V.; Veyts, I. V.; Alcock, C. B. Thermodynamic Properties of Individual Substances, Vols 1 and 2, Parts 1 and 2, Hemisphere, New York **1989**

(51) Wiedman, R. T.; Tonkyn, R. G.; White, M. G.; Wang, K.; McCoy, V. Rotationally resolved threshold photelectron spectra of OH and OD. *J. Chem. Phys.* **1992**, *97*, 768-772.

(52). Barr, J. D.; De Fanis, A.; Dyke, J. M.; Gambling, S. D.; Hooper, N.; Morris, A.; Stranges, S.; West, J. B.; Wright, T. G. Study of the OH and OD radicals with photoelectron spectroscopy using synchrotron radiation. *J. Chem. Phys.* **1999**, *110*, 345-354.

(53) Dyke, J. M.; Jonathan, N. B. H. J; Morris, A.; Winter, M. J. Vacuum ultraviolet photoelectron spectroscopy of transient species Part 13 Observation of the X^3A'' state of HO_2^+. *Mol. Phys.* **1981**, *44*, 1059-1066.

(54) NIST WebBook http://webbbook.nist.gov/chemistry/;

Figure 1.

Optimized structures of the ground state of H_2O_2 and the lowest two states of $H_2O_2^+$ (see text and Table 1).

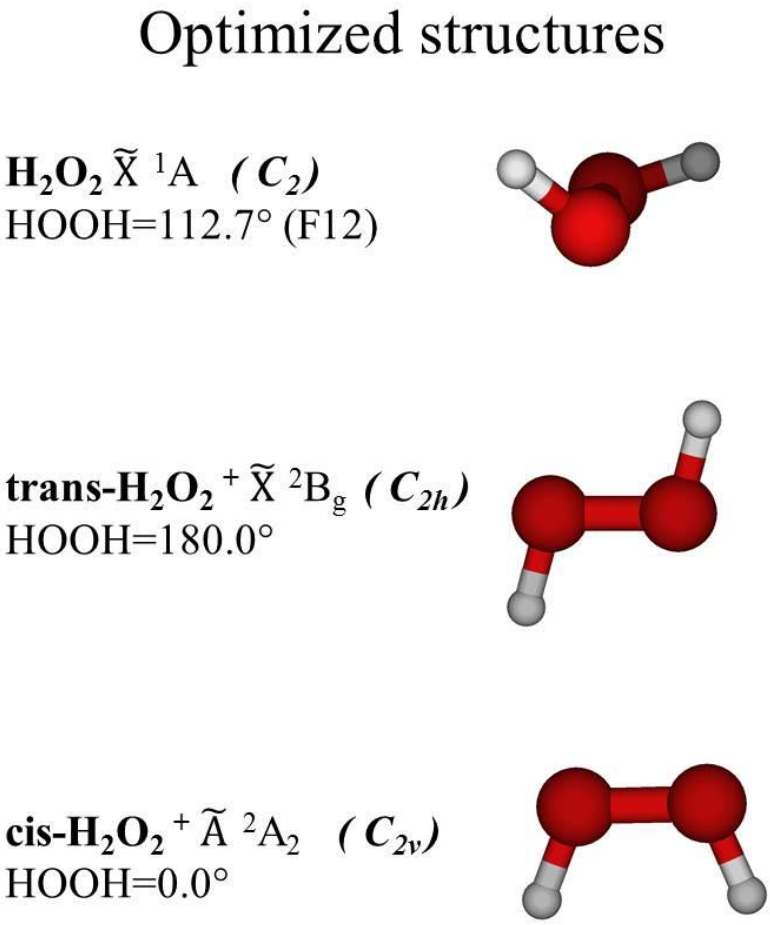

Figure 2. Computed vertical IEs by the IP-EOM CCSD method with basis set extrapolation to the CBS limit, compared with the experimental HeI PE spectrum. (The spectrum contains contributions from the HeIα, HeIβ and HeIγ $(3p)^{-1}$ $Ar^{+}(^{2}P) \leftarrow Ar(^{1}S_0)$ ionizations; these are the three sets of sharp doublet features at ~15.8; 14.0; 13.3 eV).

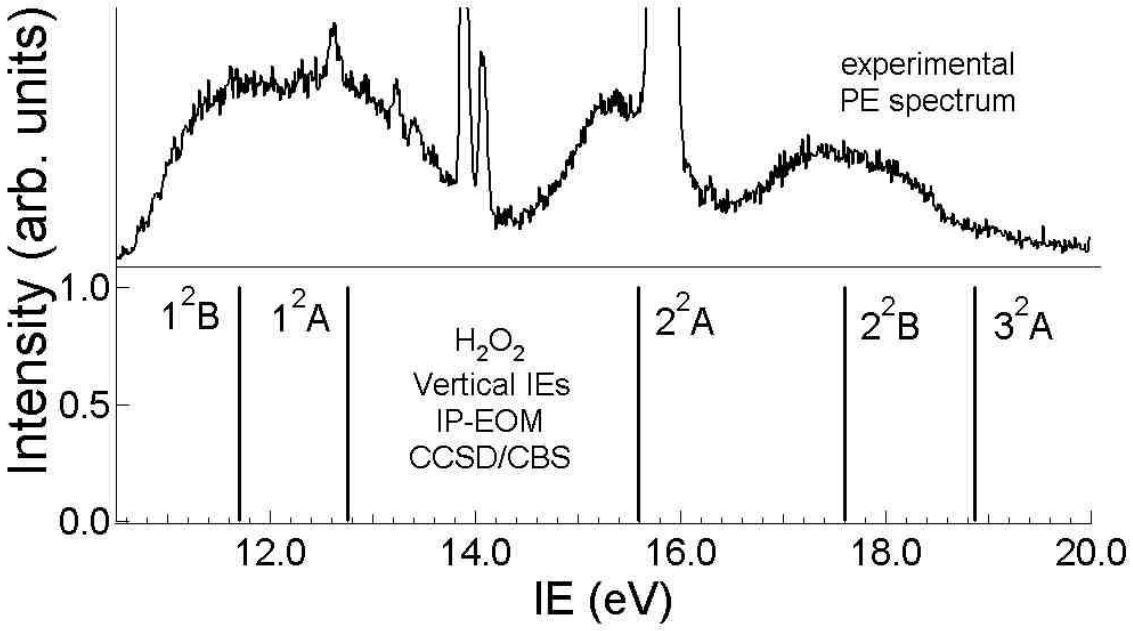

Figure 3

HeI (21.22 eV) PE spectrum of H_2O_2 in the 10.0-14.0 eV IE region.

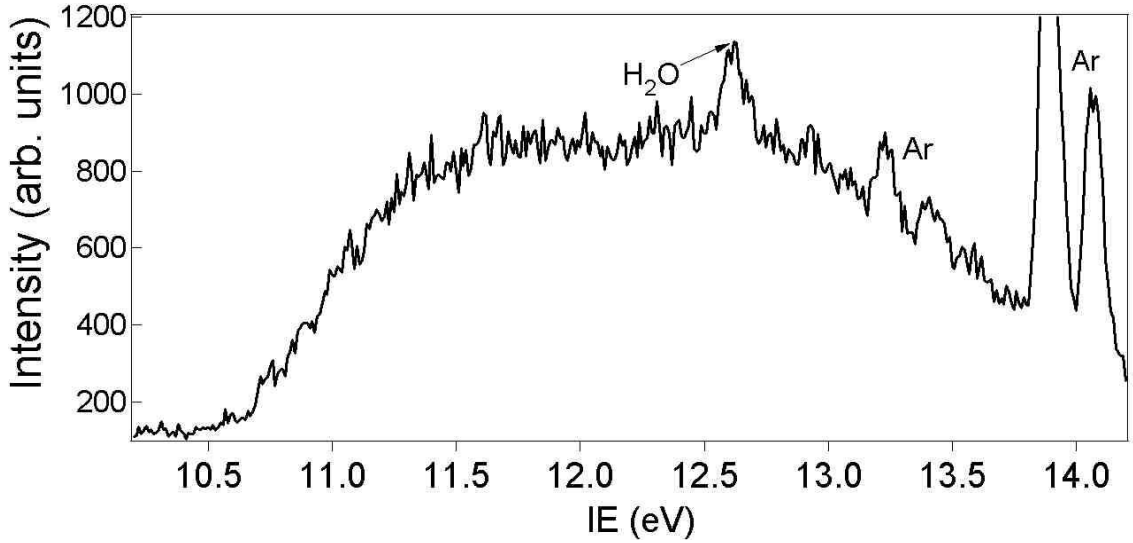

Figure 4
TPE spectrum of H_2O_2 recorded in the 10.0-20.0 eV photon energy region.

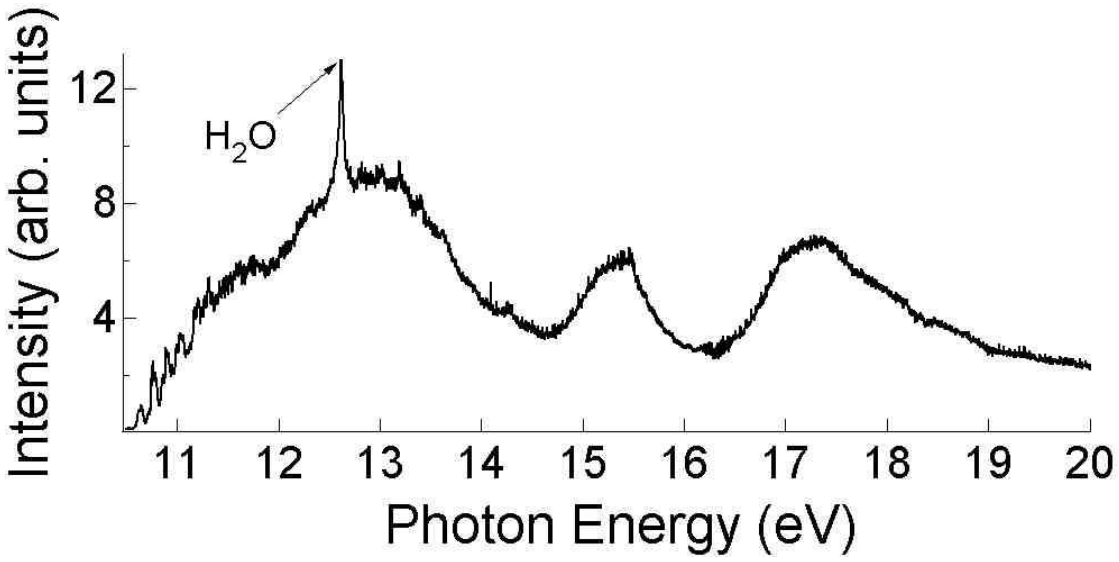

Figure 5
TPE spectrum of H_2O_2 recorded in the 10.0-14.0 eV photon energy region.

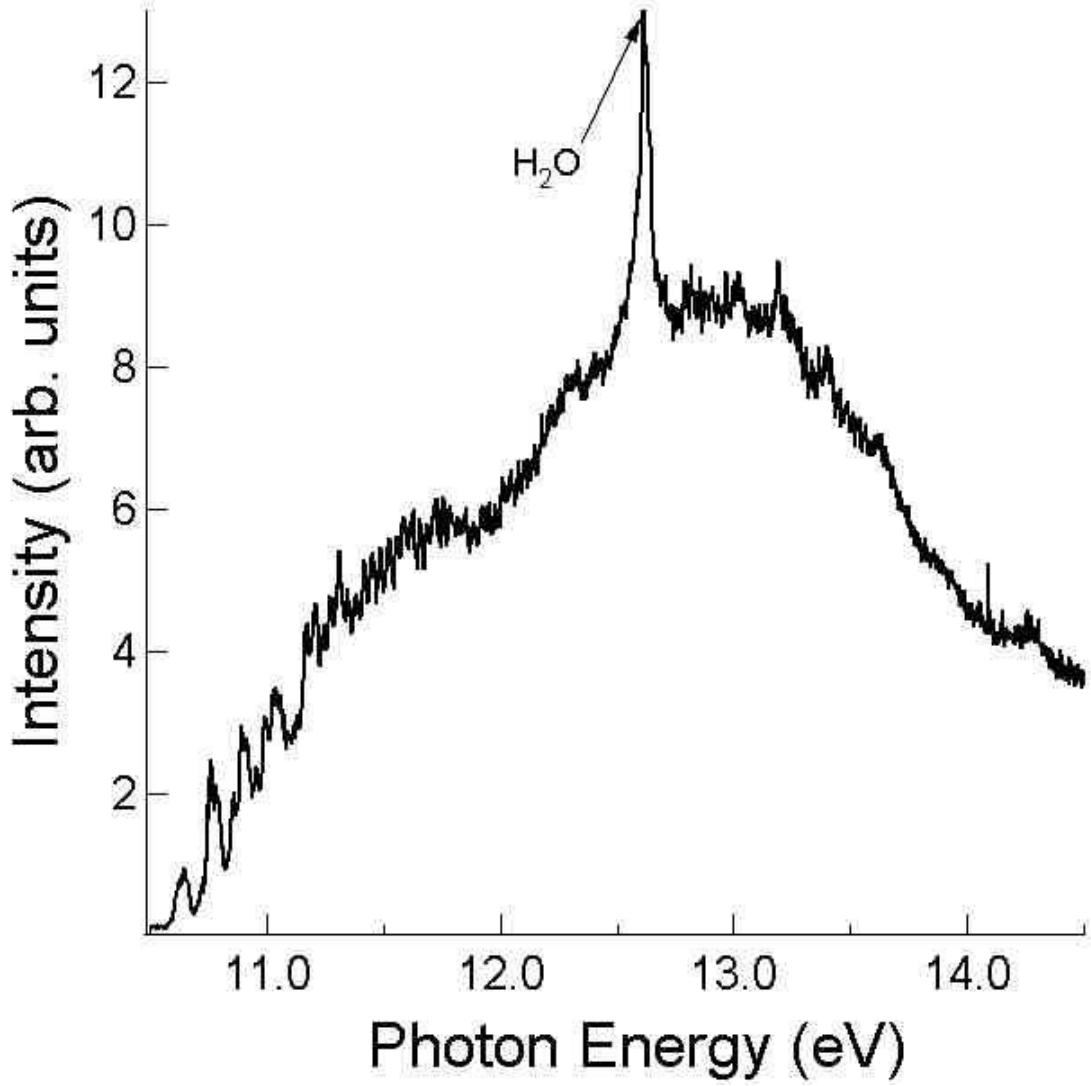

Figure 6

TPE spectrum of H_2O_2 recorded in the 10.5-12.0 eV photon energy region, showing the main resolved features in the 10.5-11.0 eV region (a, a′, a″, b, b′, b″, c).

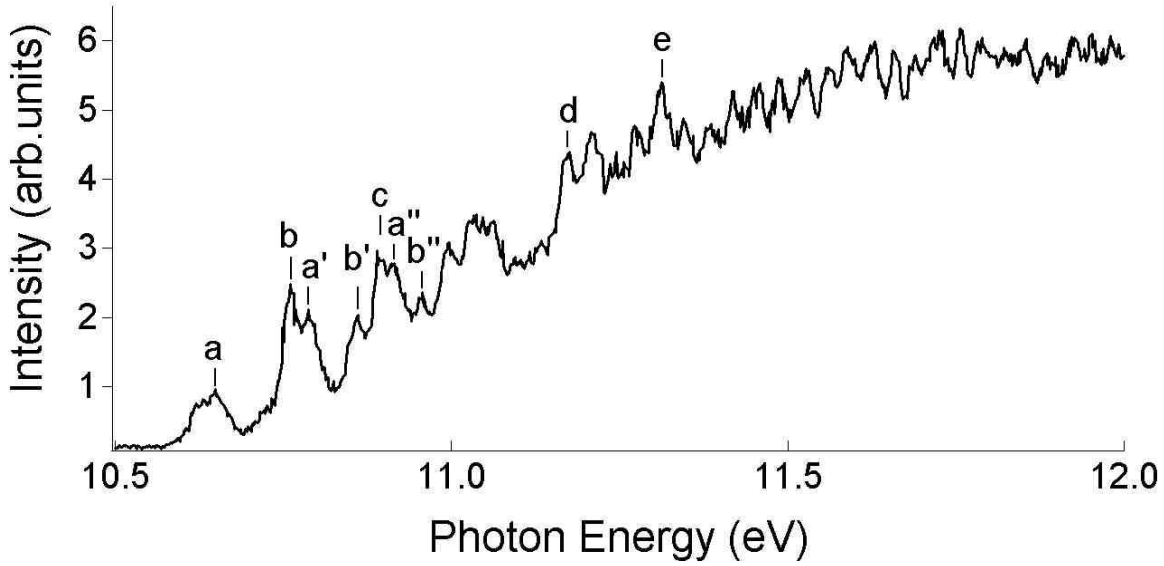

Figure 7

Comparison of the experimental TPE spectrum of H_2O_2 in the10.5-11.4 eV photon energy region with the simulated 300 K spectrum, with no 'hot-bands' from the torsional mode in the simulation. The simulated spectrum has been shifted by -0.011 eV (AIE = 10.660-0.011 = 10.649 eV; see text). Each component is simulated with a gaussian of 30 meV half-width.

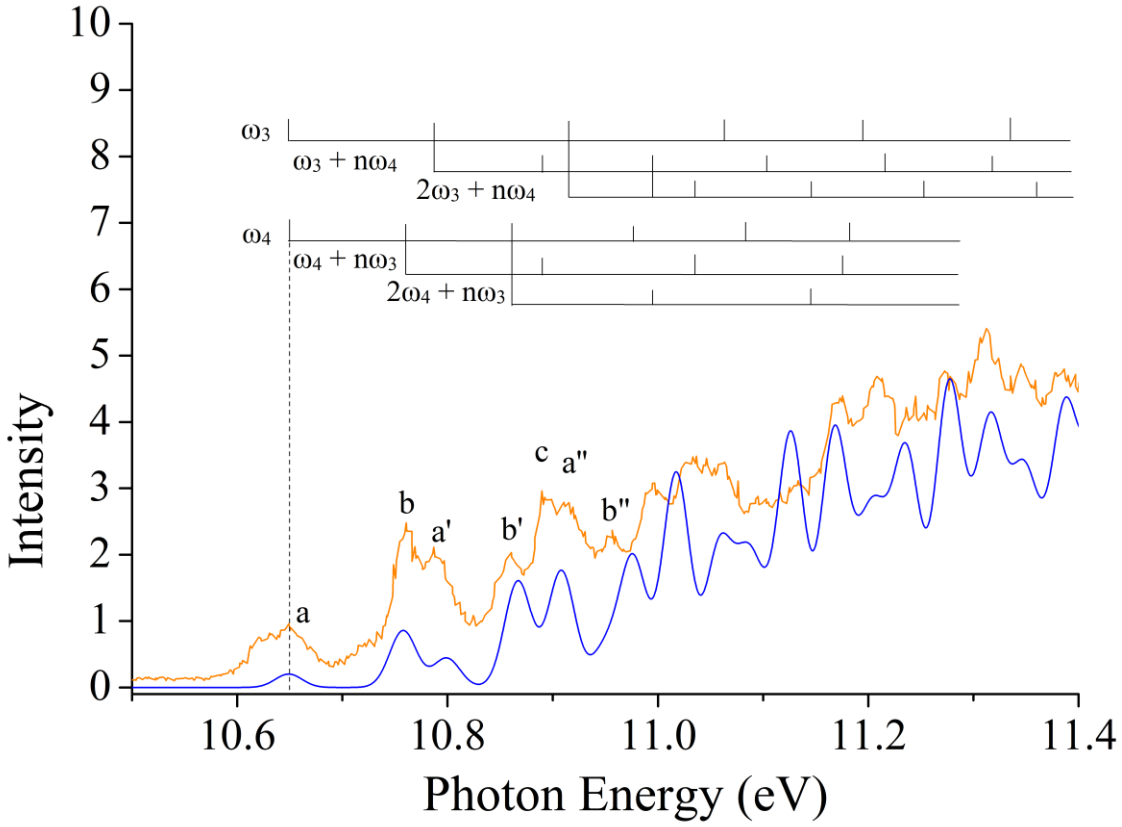

Figure 8

Comparison of the experimental TPE spectrum of H_2O_2 in the 10.5-11.4 eV photon energy region with the simulated 300 K spectrum, with no 'hot-bands' from the torsional mode in the simulation. The simulated spectrum has been shifted by +0.025 eV (AIE = 10.660+0.025 = 10.685 eV; see text). Each component is simulated with a gaussian of 30 meV half-width. The assignment of bands a, a′, a″, b, b′,b″ and c is shown in this Figure and given in the text. With this assignment, bands d and e shown in Figure 6 correspond to excitation of $3\omega_3$, $\omega_3+3\omega_4$ (d) and $4\omega_3$, $2\omega_3+3\omega_4$ (e) in the ion.

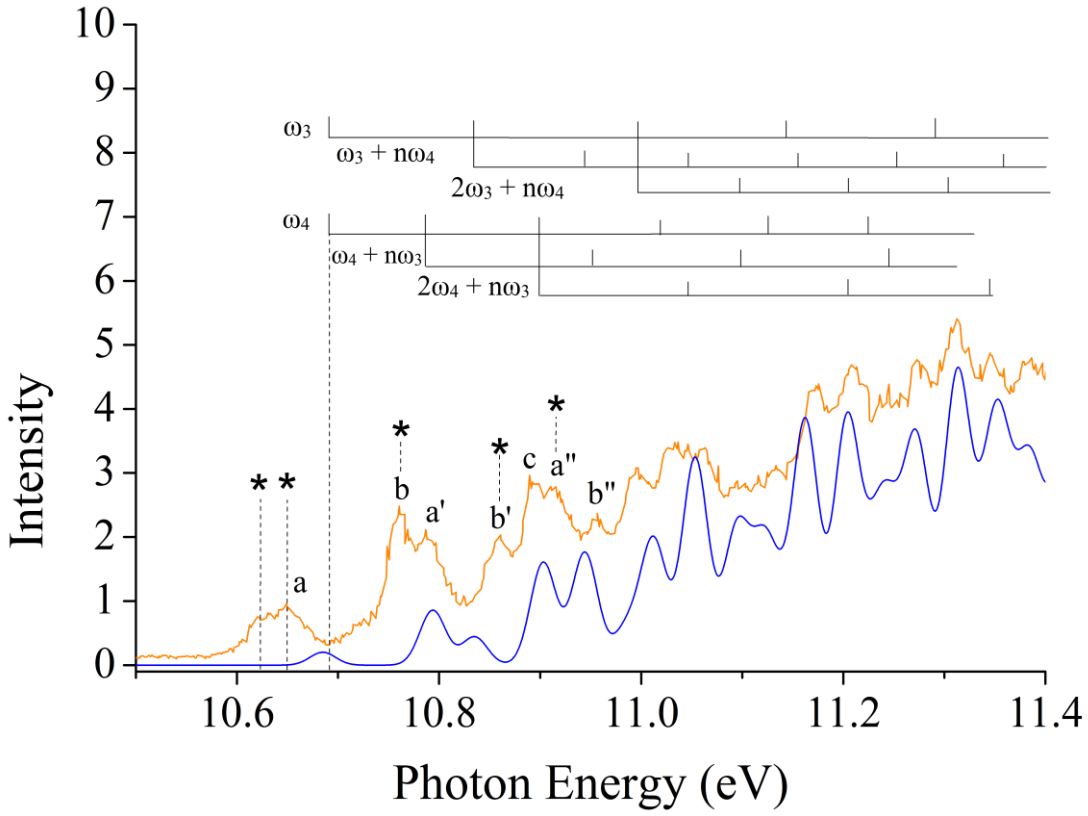

Supplementary Information

Geometrical parameters of the ground state of H_2O_2

In the early infrared work on H_2O_2 in 1962 (13), vibrationally resolved infrared spectra were recorded which gave the following rotational constants for the lowest vibrational level $A'' = 10.068$, $B'' = 0.8740$ and $C'' = 0.8384$ cm^{-1}

H_2O_2 has four structural parameters which cannot be determined from only three rotational constants. A way forward was found in ref. 13 by assuming r_0(O-H) = (0.950± 0.005) Å. Using this value, the other r_0 parameters were determined from the rotational constants as

r_0(O-O) = (1.475 ± 0.004) Å ,

∠OOH = (94.8 ± 2.0)° ,

HOOH dihedral angle = (119.8 ±3.0)°

Then using a computed r(O-H) value of (0.967 ± 0.005)Å , obtained at the MP2 level, Cremer (SI2) used the rotational constants to re-determine the other r_0 parameters as

r_0(O-O) = (1.463 ± 0.004) Å ,

∠OOH = (99.3 ± 2.0)° ,

HOOH dihedral angle = (120.2 ±3.0)°

Also, in a re-analysis of available infrared and microwave data the following r_e values were proposed (SI2, SI3), based on an assumed value of r_e (O-H) = (0.965 ± 0.005) Å,

r_e(O-O) = (1.452 ± 0.004) Å ,

∠OOH = (100.0 ± 1.0)° ,

HOOH dihedral angle = (119.2 ±1.8)°

Summary of thermodynamic values with references used to derive $\Delta H_{f,298}$ (H_2O_2), $D_{0,298}$ (HO-OH) and $D_{0,298}$(H-O_2H)

a)$\Delta H_{f,298}$ (H_2O_2)

Taken as –(32.48 ± 0.05) kcal.mol^{-1} from ref. SI3.

b) $D_{0,298}$ (HO-OH)

This is evaluated as (50.26 ± 0.23) kcal.mol^{-1} from $\Delta H_{f,298}$ (OH) = (8.89 ± 0.09) kcal.mol^{-1} (ref. SI3 and the above value of $\Delta H_{f,298}$ (H_2O_2)

c) $D_{0,298}$ (H-O_2H)

This is evaluated as (87.9 ± 0.8) kcal.mol^{-1} from $\Delta H_{f,298}$ (HO_2) = (3.3 ± 0.8) kcal.mol^{-1} , $\Delta H_{f,298}$ (H) = (52.103 ± 0.001) kcal.mol^{-1} (ref. SI3) and the above value of $\Delta H_{f,298}$ (H_2O_2)

References for SI

SI1) Cremer, D. Theoretical determination of molecular structure and conformation I. The role of basis set and correlation effects in calculations on hydrogen peroxide. *J. Chem. Phys.* **1978**, *69*, 4440-4455.

SI2) Khachkuruzov, G. A.; Przhevalskii, I. N. Molecular constants of hydrogen peroxide IV Structural parameters, *Optics and Spectroscopy* **1974**. *36*, 172-174.

SI3) Gurvich, L. V.; Veyts, I. V.; Alcock, C. B. Thermodynamic Properties of Individual Substances, Vols 1 and 2, Parts 1 and 2, Hemisphere, New York 1989.